Detecting Disease-Specific Patterns of Brain Structure Using Cortical Pattern Matching and a Population-Based Probabilistic Brain Atlas

Paul M. Thompson PhD[1], Michael S. Mega MD PhD[1], Christine Vidal[1], Judith L. Rapoport MD[2], and Arthur W. Toga PhD[1]

[1] Laboratory of Neuro Imaging, Division of Brain Mapping, and Alzheimer's Disease Center, Dept. of Neurology, UCLA School of Medicine, Los Angeles, CA, USA
thompson@loni.ucla.edu
[2] Child Psychiatry Branch, National Institute of Mental Health, Bethesda, MD, USA

Abstract. The rapid creation of comprehensive brain image databases mandates the development of mathematical algorithms to uncover disease-specific patterns of brain structure and function in human populations. We describe our construction of probabilistic atlases that store detailed information on how the brain varies across age and gender, across time, in health and disease, and in large human populations. Specifically, we introduce a mathematical framework based on covariant partial differential equations (PDEs), pull-backs of mappings under harmonic flows, and high-dimensional random tensor fields to encode variations in cortical patterning, asymmetry and tissue distribution in a population-based brain image database (N=94 scans). We use this information to detect disease-specific abnormalities in Alzheimer's disease and schizophrenia, including dynamic changes over time. Illustrative examples are chosen to show how group patterns of cortical organization, asymmetry, and disease-specific trends can be resolved that are not apparent in individual brain images. Finally, we create four-dimensional (4D) maps that store probabilistic information on the dynamics of brain change in development and disease. Digital atlases that generate these maps show considerable promise in identifying general patterns of structural and functional variation in diseased populations, and revealing how these features depend on demographic, genetic, clinical and therapeutic parameters.

1 Introduction

The widespread and rapidly accelerating collection of normal and diseased brain images *in vivo* and *ex vivo* has led to a tremendous increase in the number of investigations focusing on the structural and functional organization of the brain [1]. The complexity and variability of human brain structure across subjects is so great that mathematical algorithms are essential to effectively analyze and interpret brain data. Digital *brain atlases*, for example, represent anatomy in a 3-dimensional coordinate system. New data can be aligned with the atlas

M.F. Insana, R.M. Leahy (Eds.): IPMI 2001, LNCS 2082, pp. 488–501, 2001.

coordinate system using linear or nonlinear registration techniques [2], making it easier to pool and compare brain data from multiple subjects. Nonetheless, design of population-based brain atlases presents considerable challenges, since these systems must capture how anatomy and function vary across age and gender, in different disease states, and across imaging modalities. They must also represent these variations in such a way that systematic patterns can be identified. *Beyond Individual Atlases.* Recent developments in computational anatomy have expanded the atlas concept to store information on anatomical variation in a population [3-5]. *Deformable* brain atlases [6-8] are digital brain templates that can be elastically deformed to match the anatomy of a new subject. These atlases have powerful applications in automated image labeling [9], automated morphometry [10] and multimodality correlation [11]. They can also transfer metabolic, functional, and cytoarchitectural maps into the coordinate system of a new patient for surgical planning [12] or to relate *in vivo* functional and *post mortem* molecular hallmarks of disease [13]. Probabilistic atlases [3,14,15] store information on structural and functional variability in a population. Depending on the attribute whose statistical distribution is modeled, the information they encode can support pathology detection in an individual or group [14], or provide Bayesian prior information for tissue classification [16], image matching [8] or functional image analysis [17]. Probabilistic atlases have enormous promise in revealing the anatomical distribution and timing of clinical abnormalities in disease [18,5]. Although many diseases affect the anatomy of the cortex, there have been major difficulties in developing average and statistical representations of cortical anatomy, in view of the extreme variations in cortical patterning across subjects. Systematic differences or dynamic changes in cortical organization, gray matter distribution or asymmetry have been difficult to distinguish from normal variations, which also complicate the direct averaging of imaging data in stereotaxic space. *Goals of the Paper.* In this paper, we introduce a mathematical framework based on covariant partial differential equations (PDEs) and multivariate random tensor fields to encode variations in cortical patterning, tissue distribution and asymmetry. We build on earlier work by applying new algorithms to brain image databases from diseased populations with Alzheimer's disease and schizophrenia, including longitudinal data. We present three illustrative examples of algorithms detecting underlying patterns of disease-specific tissue loss, cortical asymmetry and dynamic brain change that are not easily identifiable in individual subjects' images. These applications suggest the potential of the approach in biomedical and clinical research settings.

2 Methods

Imaging and Subject Populations. 94 high-resolution ($256^2 \times 124$) T_1-weighted fast SPGR (spoiled GRASS) MRI volumes were acquired from four distinct subject populations: patients with Alzheimer's Disease, adolescents with schizophrenia, and their corresponding matched healthy control populations. 26 subjects with mild to moderate Alzheimer's Disease (AD; NINCDS-ARDRA criteria)

were imaged on GE Signa 1.5T clinical scanner (TR/TE 14.3/3.2 msec, flip angle 35°, NEX=1, 25cm FOV, contiguous 1.2 mm thick slices). Patients were matched for disease severity (Mini-Mental State Exam score: 20.0±0.9), and were matched for age (75.8±1.7 yrs.; 14 females/12 males), educational level (15.2±0.4 yrs.), and handedness (all right-handed) with 20 identically-imaged elderly control subjects (age: 72.4±1.3 yrs.; 8 females/12 males; education: 15.4±0.5 yrs.). A separate group of 24 subjects, recruited as part of an ongoing NIMH study of childhood-onset schizophrenia [19], were imaged longitudinally at baseline and after a 5-year interval. The 12 healthy controls (aged 13.5±0.7 years at initial scan, 18.0±0.8 years at follow-up) were age- and gender-matched with the 12 schizophrenic patients and scanned identically at exactly the same ages and intervals (patients' ages: 13.9±0.8 and 18.6±1.0 years; interval between scans: 4.6±0.3 years). Image data were *initially* transformed into a Talairach-based coordinate system [20] which (1) places the anterior commissure (AC) at the origin; (2) vertically orients the midsagittal plane; and (3) horizontally orients the AC-PC line. Aligned MR volumes were corrected for non-uniformity of MR signal intensity [16], and high-resolution surface models of the cerebral cortex were extracted, as described previously [14,21].

Mapping Cortical Patterns. To begin encoding patterns of cortical variability, parametric curves representing 36 major external fissures and sulci in the brain were manually outlined on highly magnified surface-rendered images of each cortical surface. Detailed anatomic criteria were applied as set out in [14] and the Ono sulcal atlas [22] to define sulci with consistent incidence and topology across subjects. In both brain hemispheres, 3D curves were traced to represent superior and inferior frontal, precentral, central, postcentral, intraparietal, superior and inferior temporal, primary and secondary intermediate, collateral, olfactory and occipito-temporal sulci, as well as the Sylvian fissures. Additional 3D curves represented gyral limits at the interhemispheric margin [14]. Stereotaxic locations of contour points derived from the data volumes were redigitized to produce 36 uniformly parameterized cortical contours per brain, representing each subject's primary gyral pattern.

Measuring Gyral Pattern Differences. Due to variations in gyral patterning, cortical variability is severely underestimated unless elements of the gyral pattern are matched from one subject to another (*cf.* [9,14]). This matching is also required for cortical averaging; otherwise, corresponding gyral features will not be averaged together. To find good matches among cortical regions we performed the matching process in the cortical surface's parametric space, which permits more tractable mathematics (Fig. 1; [14,23,24]). This vector flow field in the parametric space indirectly specifies a correspondence field in 3D, which drives one cortical surface into the shape of another. This mapping not only matches overall cortical geometry, but matches the entire network of the 36 landmark curves with their counterparts in the target brain, and thus is a valid encoding of cortical variation. *Maps of the Cortical Parameter Space.* Cortical models were created by driving a tiled, spherical mesh into the configuration of each subject's cortex [25,21,26], so any point on the cortical surface must map to exactly one

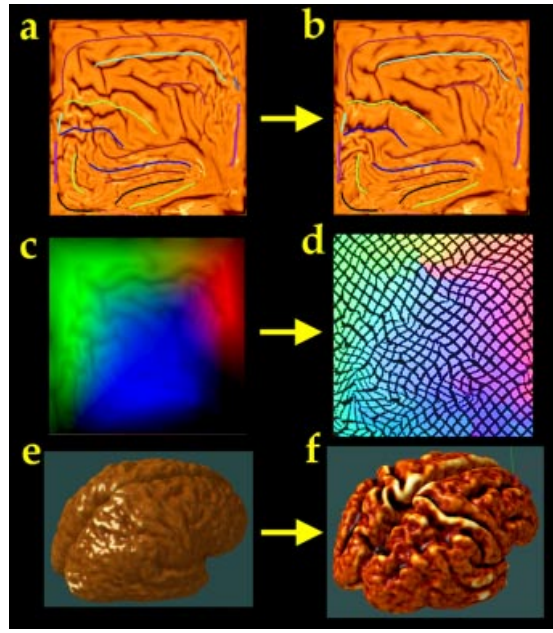

Fig. 1. Averaging Cortical Models. A well-resolved average cortical model (f) for a group of subjects can be created by first flattening each subject's cortical model to a 2D square (a). A color coded map (c) stores a unique color triplet (RGB) at each location in the 2D parameter space encoding the (x,y,z) coordinate of the 3D cortical point mapped to that 2D location. However, a well-resolved average model (f) is produced, with cortical features in their group mean location, if each subject's color map is first flowed (d) so that sulcal features are driven into the configuration of a 2D average sulcal template (b). Codes indexing similar 3D anatomical features are placed at corresponding locations in the parameter space, and are thus reinforced in the group average (f).

point on the sphere and *vice versa*. Each cortical surface is parameterized with an invertible mapping D_p,D_q: (r,s)→(x,y,z), so sulcal curves and landmarks in the folded brain surface can be reidentified in a spherical map (*cf.* [24]). To retain relevant 3D information, cortical surface point position vectors (x,y,z) in 3D stereotaxic space were color-coded using a unique RGB color triplet, to form an image of the parameter space in color image format (Fig. 1). These spherical locations, indexed by two parameters, can also be mapped to a plane (Fig. 1; [14]). Cortical differences between any pair of subjects were calculated as follows. A flow field was first calculated that elastically warps one flat map onto another from the other subject (Fig. 1; or equivalently, one spherical map onto the other). On the sphere, the parameter shift function $\mathbf{u}(\mathbf{r}):\Omega \rightarrow \Omega$, is given by the solution $F_{pq}:\mathbf{r}\rightarrow\mathbf{r}\text{-}\mathbf{u}(\mathbf{r})$ to a curve-driven warp in the spherical parametric space $\Omega=[0,2\pi)\times[0,\pi)$ of the cortex (Fig. 1; [14]). For points $\mathbf{r}=(r,s)$ in the

parameter space, a system of simultaneous partial differential equations can be written for the flow field $\mathbf{u}(\mathbf{r})$:

$$L^{\sharp}(\mathbf{u(r)}) + \mathbf{F}(\mathbf{r\text{-}u(r)}) = \mathbf{0}, \forall \mathbf{r} \in \Omega, \text{ with } \mathbf{u}(\mathbf{r}) = \mathbf{u_0}(\mathbf{r}), \forall \mathbf{r} \in M_0 \cup M_1. \quad (1)$$

Here M_0, M_1 are sets of points and (sulcal or gyral) curves where displacement vectors $\mathbf{u}(\mathbf{r})=\mathbf{u_0}(\mathbf{r})$ matching corresponding anatomy across subjects are known. The flow behavior is modeled using equations derived from continuum mechanics, and these equations are governed by the Cauchy-Navier differential operator $L = \mu\nabla^2+(\lambda+\mu)\nabla(\nabla^T \bullet)$ with body force $\mathbf{F}$ [14,27,4]. The only difference is that $L^{\sharp}$ is the *covariant* form of the differential operator L (for reasons explained below[1]). This approach not only guarantees precise matching of cortical landmarks across subjects, but creates mappings that are independent of the surface metrics, and therefore independent of the surface parameterizations. *Cortical Averaging using Pull-backs and Flows in Parameter Space.* The intersubject variability of the

[1] **Covariant Mapping Equations**. Since the cortex is not a *developable* surface, it cannot be given a parameterization whose metric tensor is uniform. As in fluid dynamics or general relativity applications, the intrinsic curvature of the solution domain can be taken into account when computing flow vector fields in the cortical parameter space, and mapping one mesh surface onto another. In the *covariant tensor* approach [4], correction terms (Christoffel symbols, $\Gamma^{\mathbf{i}}_{\mathbf{jk}}$) make the necessary adjustments for fluctuations in the metric tensor of the mapping procedure. In the partial differential equations (1), we replace L by the covariant differential operator $L^{\sharp}$. In $L^{\sharp}$, all L's partial derivatives are replaced with *covariant* derivatives [28]. These covariant derivatives are defined with respect to the metric tensor of the surface domain where calculations are performed. The covariant derivative of a (contravariant) vector field, $u^i(\mathbf{x})$, is defined as $u^i{}_{,k} = \partial u^j/\partial x^k + \Gamma^{\mathbf{j}}_{\mathbf{ik}}\, u^i$ where the *Christoffel symbols of the second kind* [28], $\Gamma^{\mathbf{j}}_{\mathbf{ik}}$, are computed from derivatives of the metric tensor components $g_{jk}(\mathbf{x})$:

$$\Gamma^{\mathbf{i}}_{\mathbf{jk}} = (1/2)\; g^{il}\; (\partial g_{lj}/\partial x^k + \partial g_{lk}/\partial x^j - \partial g_{jk}/\partial x^i). \quad (2)$$

These correction terms are then used in the solution of the Dirichlet problem [29] to match one cortex with another. Note that a parameterization-invariant variational formulation could also be used to minimize metric distortion when mapping one surface to another. If P and Q are cortical surfaces with metric tensors $g_{jk}(u^i)$ and $h_{jk}(\xi^\alpha)$ in local coordinates u^i and ξ^α (i, α=1,2), the *Dirichlet energy* of the mapping $\xi(u)$ is defined as: $E(\xi) = \int_{\mathbf{P}} e(\xi)(u)\, dP$, where $e(\xi)(u) = g^{ij}(u)\, \partial\xi^\alpha(u)/\partial u^i\; \partial\xi^\beta(u)/\partial u^j\; h_{\alpha\beta}(\xi(u))$ and $dP=(\sqrt{det[g_{ij}]})\; du^1\, du^2$. The Euler equations, whose solution $\xi^\alpha(u)$ minimizes the mapping energy, are:

$$0 = L(\xi^i) = \Sigma_{m=1to2}\; \partial/\partial u^m\; [(\sqrt{det[g^{ru}]}\;)\; \Sigma_{l=1to2}\; g^{ml}{}_{ur}\; \partial\xi^i/\partial u^l\;]\; (i{=}1,2), \quad (3)$$

[30]. The resulting (harmonic) map (1) minimizes the change in metric from one surface to the other, and (2) is again independent of the parameterizations (spherical or planar) used for each surface. [Related algorithms for minimizing harmonic energies, invariant under reparameterization, have been developed in modeling liquid crystals [31] and in Polyakov's formulation of string theory [32]].

cortex is computed by first creating an average cortex for each subject group and measuring individual differences from the deformation mappings that drive the average model onto each individual. By defining probability distributions on the space of deformation transformations applied to the average template [4], statistical parameters of these distributions are estimated from the databased anatomic data to determine the magnitude and directional biases of anatomic variation. To do this, all 36 gyral curves for all subjects are first transferred to the parameter space. Next, each curve is uniformly re-parameterized to produce a regular curve of 100 points whose corresponding 3D locations are uniformly spaced. A set of 36 average gyral curves for the group is created by vector averaging all point locations on each curve. This *average curve template* (*curves* in Fig. 1(a)) serves as the target for alignment of individual cortical patterns [24]. Each individual cortical pattern is transformed into the average curve configuration using a flow field in the parameter space (Fig. 1(b); *cf.* [33]). By carrying a color code (that indexes 3D locations; Fig. 1(c)) along with the vector flow that aligns each individual with the average folding pattern, information can be recovered at a particular location in the average folding pattern (Fig. 1(d)) specifying the 3D cortical points mapping each subject to the average. In the language of Lie algebras, corresponding 3D cortical points across the subject database are defined as the *pull-back* $D_p{}^*(\mathbf{r})$ [28] of the parameterization mappings D_p: (r,s)→(x,y,z) under the covariant vector flow $\mathbf{u}(\mathbf{r})$ that maps each subject to the average curve template. [For any smooth function D_p: $\Omega \rightarrow R^n$ and any diffeomorphic map $\mathbf{u}(\mathbf{r})$: $\Omega \rightarrow N$, there is a function on N, $D_p{}^*$: $N \rightarrow R^n$ called the pull-back of D_p by $\mathbf{u}(\mathbf{r})$, and defined by $D_p \circ \mathbf{u}$ [28]]. This produces a new coordinate grid [the *pull-back* $D_p{}^*(\mathbf{r})$; Fig. 1(d)] on a given subject's cortex in which particular grid-points appear in the same location across subjects relative to the mean gyral pattern. By averaging these 3D positions across subjects, an average 3D cortical model can be constructed for the group. An example of this type of cortical average, based on 9 subjects with Alzheimer's disease, is shown in Fig. 1(f). The resulting mapping is guaranteed to average together all points falling on the same cortical locations across the set of brains, and ensures that corresponding features are averaged together.

Affine Shape Adjustment. Prior to generating an average cortex, an average image template is generated with the average affine shape for the subjects in the group, and individual scans are globally aligned to this template. This is done so that (1) differences in global brain scale and affine position are factored out before computation of variability, and (2) measurements are made and maps generated at the mean spatial scale for the group. To produce a template with the mean image intensity and geometry for the group, a subset of brains was selected for which a comprehensive set of anatomic surface models had been created (84 per brain), including models of deep brain structures [34]. An initial image template for the group was constructed by (1) using automated linear transformations [35] to align the MRI data with a randomly selected image, (2) intensity-averaging the aligned scans, and then (3) recursively re-registering the scans to the resulting average affine image. The resulting average image was

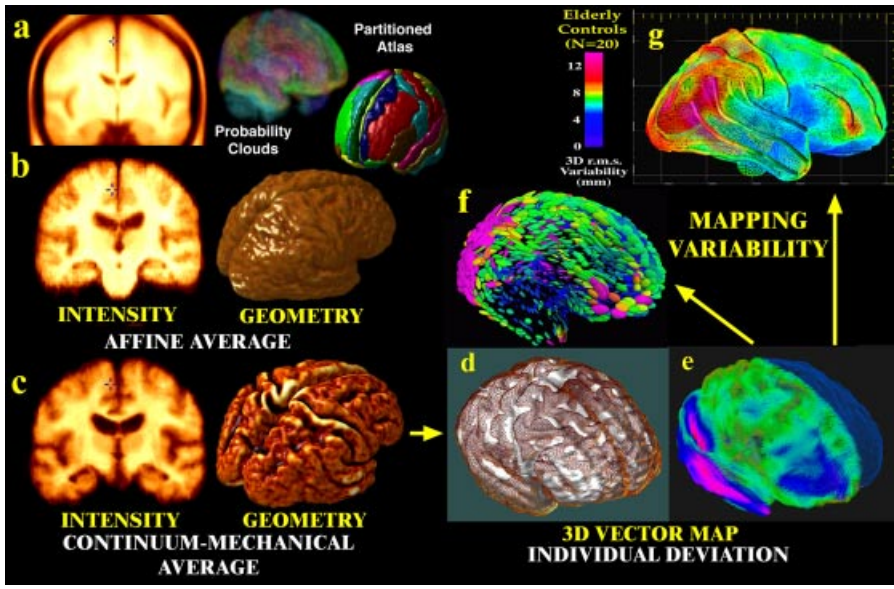

Fig. 2. Probabilistic Modeling of Brain Anatomy. Direct averaging of imaging data after a simple affine transform into stereotaxic space washes cortical features away ((a); Evans et al., 1994; N=305 normals); (b) a similar approach with N=9 Alzheimer's patients). By first averaging a set of vector-based 3D geometric models, and warping each subject's scan into the average configuration, a well-resolved average brain template is produced (c). Deformation vector maps (e) store individual deviations (*brown mesh*) from a group average (*white surface*, (d)), and their covariance fields (f) store information on the preferred directions and magnitude (g) of anatomic variability (*pink colors, large variation; blue colors, less*).

adjusted to have the mean affine shape for the group, using matrix logarithms for transformation averaging and exponentiation [35]. Images and surface models were then linearly aligned to this template, and an average surface set was created for the group [34]. Displacement maps (Fig. 2(e)) driving the surface anatomy of each subject into correspondence with the average surface set were then extended to the full volume with a 3D warping algorithm based on surface-driven elasticity [14,25,27]. These warping fields reconfigured each subject's 3D image into the average anatomic configuration for the group. By averaging the reconfigured images (after intensity normalization), a crisp image template was created to represent the group (Fig. 2(c)). Note the better-resolved cortical features in the average images after high-dimensional cortical registration (Fig. 2(c)). If desired, this AD-specific atlas can retain the coordinate matrix of the Talairach system (with the anterior commissure at (0,0,0)) while refining the gyral map of the Talairach atlas to encode the unique anatomy of the AD popu-

lation. By explicitly computing matching fields that relate gyral patterns across subjects, a well-resolved and spatially consistent set of probabilistic anatomical models and average images can be generated to represent the average anatomy and its variation in a subpopulation.

3 Results

Tensor Maps of 3D Cortical Variation. By using cortical pattern matching to identify corresponding cortical locations in 3D space, rather than simple image averaging (Fig. 2(a),(b)), deformation maps can be recovered mapping each patient into gyrus-by-gyrus correspondence with the average cortex (Fig. 2(e)). Anatomic variability can thus be defined at each point on the average cortical mesh as the root mean square magnitude of the 3D displacement vectors, assigned to each point, in the surface maps from individual to average. This variability pattern is visualized as a color-coded map (Fig. 2(g)). This map shows the anatomic differences, due to gyral pattern variation, that remain after affine alignment of MR data into a brain template with the mean shape and intensity for the group. After these affine components of the deformation fields are factored out, the deformation vector required to match the structure at position $\mathbf{x}$ in the average cortex with its counterpart in subject i can be modeled as:

$$\mathbf{W}_i(\mathbf{x}) = \mu(\mathbf{x}) + \Sigma(\mathbf{x})^{1/2}\epsilon_i(\mathbf{x}). \quad (4)$$

Here $\mu(\mathbf{x})$ is the mean deformation vector for the population (which approaches the zero vector for large N), $\Sigma(\mathbf{x})$ is a non-stationary, anisotropic covariance tensor field estimated from the mappings, $\Sigma(\mathbf{x})^{1/2}$ is the upper triangular Cholesky factor tensor field, and $\epsilon_i(\mathbf{x})$ can be modeled as a trivariate random vector field whose components are independent zero-mean, unit variance, stationary random fields. This 3D probability distribution makes it possible to visualize the principal directions (eigenvectors) as well as the magnitude of gyral pattern variability, and these characteristics are highly heterogeneous across the cortex. For any desired confidence threshold α, 100(1-α)% *confidence regions* for possible locations of points corresponding to $\mathbf{x}$ on the average cortex are given by nested ellipsoids $\mathbf{E}_{\lambda(\alpha)}(\mathbf{x})$ in displacement space (Fig. 2(f)).

Here

$$\mathbf{E}_\lambda(\mathbf{x}) = \{\mu(\mathbf{x}) + \lambda[\Sigma(\mathbf{x})]^{-1/2}\mathbf{p} | \forall \mathbf{p} \in \mathbf{B}(\mathbf{0}; 1)\}, (5)$$

where $\mathbf{B}(\mathbf{0}; 1)$ is the unit ball in R^3, and

$$\lambda(\alpha) = [[N(N-3)/3(N^2-1)]^{-1} F_{\alpha,3,N-3}]^{1/2}, (6)$$

where $F_{\alpha,3,N-3}$ is the critical value of the F distribution such that $Pr\{F_{3,N-3} \geq F_{\alpha,3,N-3}\} = \alpha$ and N is the number of subjects. *Mean Asymmetry.* By analysis of variance in 3D deformation fields that match different subjects' anatomies, it is also possible to differentiate intra-subject (between hemisphere), inter-subject,

and inter-group contributions to brain variation in human populations, and detect significant differences using null distributions for features in Hotelling's T^2 random fields [14,36,37]. Mapping the pattern of brain asymmetry in a group is an interesting application. Although the set of mappings computed so far specifies the set of cortical points that correspond across subjects, the mean asymmetry cannot yet be computed without an additional set of mappings to define the points that correspond across hemispheres. To do this, all left hemisphere sulcal curves are projected into the cortical parameter space, reflected in the vertical axis, and averaged with their flattened counterparts in the right hemisphere, to produce a second *average curve template*. Color maps (Fig. 1(c)) representing point locations in the left and right hemispheres are then subjected to a second covariant flow that transforms corresponding features in each hemisphere to the same location in parameter space. 3D deformation fields can then be recovered matching each brain hemisphere with a reflected version of the opposite hemisphere (cf. [36]). The parameter flows are advantageous in that the asymmetry fields are also *registered*; in other words asymmetry measures can be averaged across corresponding anatomy at the cortex. This is not necessarily the case if warping fields are averaged at the same coordinate locations in stereotaxic space (cf. Fig. 1(a)). The pattern of mean brain asymmetry for a group of 20 subjects is shown in Fig. 3. The resulting asymmetry fields $\mathbf{a}_i(\mathbf{r})$ (at parameter space location $\mathbf{r}$ in subject i) were treated as observations from a spatially-parameterized random vector field [14,36], with mean $\mu_{\mathbf{a}}(\mathbf{r})$ and a non-stationary covariance tensor $\Sigma_{\mathbf{a}}(\mathbf{r})$ (Fig. 3(c)). The significance α of deviations from symmetry can be assessed using a T^2 or F statistic that indicates evidence of significant asymmetry in cortical patterns between hemispheres:

$$\alpha(\mathbf{r}) = F^{-1}_{3,N-3}\left([(N\text{-}3)/3(N\text{-}1)]\mathrm{T}^2(\mathbf{r})\right)$$
$$\text{where } \mathrm{T}^2(\mathbf{r}) = N[\mu_{\mathbf{a}}(\mathbf{r})^T \ {\Sigma_{\mathbf{a}}}^{-1}(\mathbf{r}) \ \mu_{\mathbf{a}}(\mathbf{r})]. \quad (7)$$

Multiple Comparisons Correction. By calculating these statistics, and their corresponding significance values (p-values), at each lattice location across a parameterized 3D anatomical surface, a statistic image is formed (Fig. 3(d)). To assess the significance of the effect, analytical null distributions have been derived for the number and extent of signal components that are likely to occur by accident above a given threshold in a statistic image, such as a T^2-distributed random field on a manifold. Because these formulae require the residuals of the statistical model to be stationary and isotropic [38,39], we adopted a non-parametric approach. A null distribution for the area of the T^2 statistic image above a fixed high threshold on the average cortical surface was computed empirically by permutation of the covariate vector (here a binary vector coding for hemisphere) and conducting 1,000,000 randomizations. By reference to this null distribution, the significance of the asymmetry was found to be $p < 0.01$.

Gray Matter Loss in a Diseased Population. A second application was to reveal the average profile of gray matter loss across the cortex in Alzheimer's disease, based on a large number of subjects at a specific stage in the disease. Gyral pattern variation makes it difficult to make inferences if gray matter maps

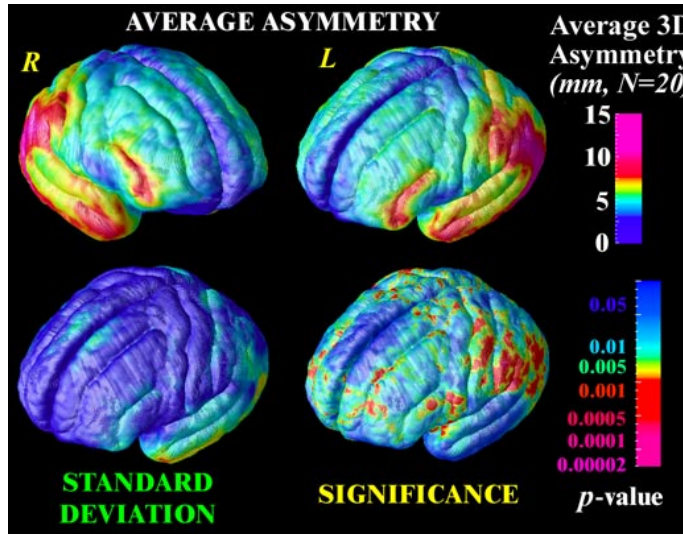

Fig. 3. Mapping Brain Asymmetry in a Population. The average magnitude of brain asymmetry in a group (N=20, elderly normals) can be assessed based on warping fields that map the cortical pattern of one hemisphere onto the other, and then flow the observations again so that corresponding measures can be averaged across subjects. Variations in asymmetry are also non-stationary across the cortex (*lower left*), and a Hotelling's T^2 statistical field can be computed to map the significance of the asymmetry (*lower right*) relative to normal anatomic variations.

are directly averaged together in stereotaxic space (e.g., Fig. 1(a)), and the ability to localize results to specific cortical regions is also lost. To address this, we used covariant flows to assist in computing group averages and statistics. First, we segmented all images in the database with a previously validated Gaussian mixture classifier. Maps of gray matter, white matter, CSF and a background class were created for each subject (Fig. 4). The proportion of gray matter lying within 15 mm of each cortical point was then plotted as an attribute on each cortex, and aligned across subjects by projecting it into flat space (Fig. 1(c)) and warping the resulting attribute field with the elastic matching technique (as in Fig. 1(d)). (Again, the gray matter proportion can be thought of as a scalar attribute $G(\mathbf{r})$ defined in the cortical parameter space, which can be subjected to a *pull-back* with the flow field $\mathbf{u}(\mathbf{r})$ to compensate for gyral pattern differences). By averaging the aligned maps, and texturing them back onto a group average model of the cortex, the average magnitude of gray matter loss was computed for the Alzheimer's disease population (Fig. 4). Regions with up to 30% reduction in the measure were sharply demarcated from adjacent regions with little or no loss. The group effect size was measured by attaching a field of t statistics, $t(\mathbf{r})$, to the cortical parameter space, and computing the area of

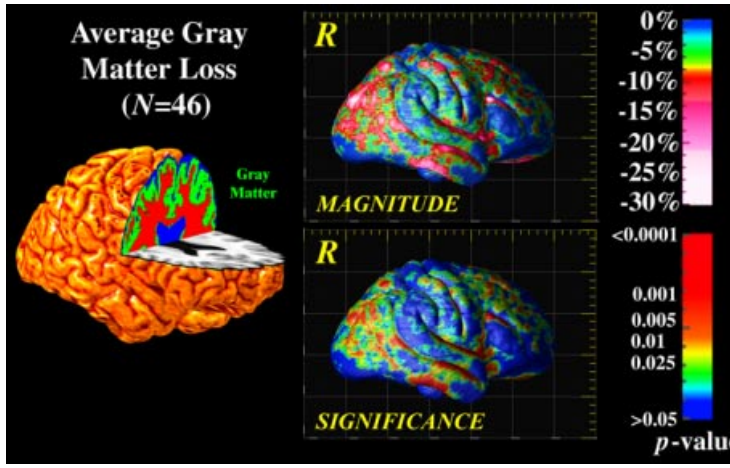

Fig. 4. Mapping Gray Matter Loss in a Population. Scalar fields that represent the distribution of gray matter across the cortex can be aligned using elastic matching of cortical patterns. A localized and highly significant loss of gray matter is revealed in temporo-parietal cortices of Alzheimer's patients relative to matched elderly controls, in a similar pattern to the metabolic and perfusion deficits seen early in the disease.

the t field on the group average cortex above a fixed threshold ($p < 0.01$, uncorrected). In a multiple comparisons correction, the significance of the overall effect was confirmed to be $p < 0.01$, by permuting the assignment of subjects to groups 1,000,000 times. (The resulting $46 \times 65536 \times 10^6 \cong 3.0 \times 10^{12}$ linear regressions - for 46 subjects, 65,536 cortical points, and 10^6 permutations - were run in parallel on an SGI *RealityMonster* with 32 R10000 180MHz internal CPUs, requiring 33 CPU hours in total). *Dynamic Brain Change.* In a third application, the same procedure was applied to longitudinal MRI data from 12 schizophrenic patients and 12 adolescent controls scanned at both the beginning and end of a 5-year interval. The goal was to estimate the average rate of gray matter loss at the cortex, by matching cortical patterns and comparing changes in disease with normal changes in controls. Cortical models and gray matter measures were elastically matched first within each subject across time, to compute individual rates of loss, and then flowed into an average configuration using flat space warping (Fig. 1(d)). The resulting maps (Fig. 5) suggested dynamic loss of gray matter in superior parietal, motor and frontal brain regions (up to 5% annually), and the group differences were highly significant ($p < 0.01$, *permutation test;* Fig. 5(b)). *Conclusion.* Atlasing of brain data from large human populations presents major challenges because of the need to compare or integrate imaging data from subjects whose anatomy is different. Although direct averaging of data in stereotaxic space may be ideal for many applications, group patterns in brain structure or function may go unnoticed because cortical regions are not well-aligned across

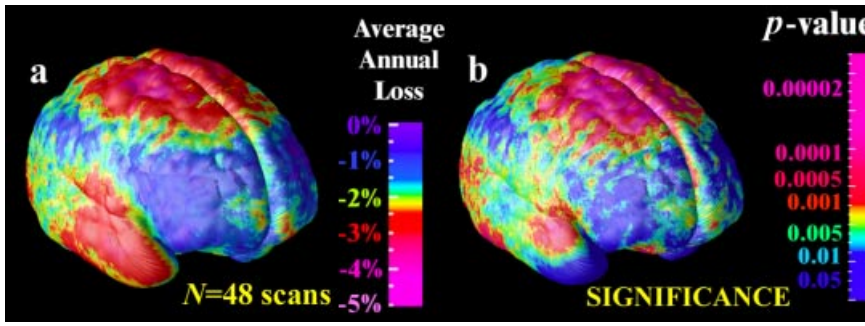

Fig. 5. Dynamic Rates of Gray Matter Loss in a Population. Scalar fields representing the rates of gray matter loss in individuals with schizophrenia can be aligned and compared with age-matched controls. Adolescents with schizophrenia experience statistically higher rates of loss in motor, frontal and temporal regions.

subjects. We presented an approach that allows the generation of well-resolved average brain maps that accommodate the wide variations in cortical patterning. By capturing variations in cortical attributes and cortical geometry using separate statistical fields, general features of cortical organization also emerged, such as the consistent pattern of brain asymmetry in perisylvian cortices (Fig. 3). Finally, by mapping gray matter differences or dynamic changes in diseased populations with Alzheimer's disease and schizophrenia, we resolved general features of the disease process that may be hard to identify in individual scans. The resulting atlasing techniques show promise in elucidating the dynamics of disease in human populations, and their relationship to genetic, cognitive, or therapeutic factors.

Acknowledgements

This work was generously supported by research grants from the National Center for Research Resources (RR13642), National Library of Medicine (LM/MH05639), NINDS (NS38753), the National Science Foundation (BIR 93-22434) and by a Human Brain Project grant known as the International Consortium for Brain Mapping, which is funded jointly by NIMH and NIDA (P20 MH/DA52176).

References

1. Fox PT (1997). The Growth of Human Brain Mapping, Hum. Br. Mapp. 5(1):1-2.
2. Toga AW (1998). Brain Warping, Academic Press.
3. Mazziotta JC, Toga AW, Evans AC, Fox P, Lancaster J (1995). A Probabilistic Atlas of the Human Brain: Theory and Rationale for its Development, NeuroImage 2: 89-101.

4. Grenander U, Miller MI (1998). Computational Anatomy: An Emerging Discipline, Technical Report, Dept. of Mathematics, Brown University.
5. Thompson PM, Mega MS, Toga AW (2000). Disease-Specific Brain Atlases, in Mazziotta JC et al., [eds.], Brain Mapping: The Disorders, Academic Press.
6. Bajcsy R, Kovacic S (1989). Multiresolution Elastic Matching, Computer Vision, Graphics and Image Processing, 46:1-21.
7. Christensen GE, Rabbitt RD, Miller MI (1996). Deformable Templates using Large Deformation Kinematics, IEEE Trans. on Image Processing 5(10):1435-1447.
8. Gee JC, LeBriquer L, Barillot C, Haynor DR, Bajcsy R (1995). Bayesian Approach to the Brain Image Matching Problem, Inst. for Res. in Cogn. Sci. Tech. Report 95-08.
9. Collins DL, Le Goualher G, Venugopal R, Caramanos A, Evans AC, Barillot C (1996). Cortical Constraints for Non-Linear Cortical Registration, In: Höhne KH, Kikinis R, [eds.], VBC'96, Hamburg, SPIE vol. 1131:307-316.
10. Ashburner J, Hutton C, Frackowiak R, Johnsrude I, Price C, Friston K (1998). Identifying global anatomical differences: deformation-based morphometry. Hum. Brain Mapping 1998;6(5-6):348-57.
11. Toga AW, Thompson PM (1998). Multimodal Brain Atlases, Chapter in: Medical Image Databases, Wong STC [ed.], Kluwer Academic, 53-88.
12. Kikinis R, Shenton ME, Iosifescu DV, McCarley RW, Saiviroonporn P, Hokama HH, Robatino A, Metcalf D, Wible CG, Portas CM, Donnino R, Jolesz F (1996). A Digital Brain Atlas for Surgical Planning, Model-Driven Segmentation, and Teaching, IEEE Trans. on Visualization and Comp. Graphics, Sept. 1996, 2(3):232-241.
13. Mega MS, Chen S, Thompson PM, Woods RP, Karaca TJ, Tiwari A, Vinters H, Small GW, Toga AW (1997) Mapping Pathology to Metabolism: Coregistration of Stained Whole Brain Sections to PET in Alzheimer's Disease, NeuroImage **5**:147-153.
14. Thompson PM, MacDonald D, Mega MS, Holmes CJ, Evans AC, Toga AW (1997). Detection and Mapping of Abnormal Brain Structure with a Probabilistic Atlas of Cortical Surfaces, J. Comp. Assist. Tomogr. 21(4):567-581, Jul.-Aug. 1997.
15. Fox PT, Mikiten S, Davis G, Lancaster JL (1994). BrainMap: A Database of Human Functional Brain Mapping, in: Functional Neuroimaging: Technical Foundations, Thatcher RW, Hallett M, Zeffiro T, John ER, Huerta M [eds.], 95-106.
16. Sled JG, Zijdenbos AP, Evans AC (1998). A non-parametric method for automatic correction of intensity non-uniformity in MRI data, IEEE Transactions on Medical Imaging, vol. 17, no. 2, Feb.1998.
17. Dinov ID,Mega MS, Thompson PM, Lee L, Woods RP, Holmes CJ, Sumners DW, Toga AW (2000) Analyzing Functional Brain Images in a Probabilistic Atlas: A Validation of Sub-Volume Thresholding, J. Comp. Assist. Tomography [in press].
18. Zijdenbos A, Evans A, Riahi F, Sled J, Chui H-C, Kollokian V (1996). Automatic quantification of multiple sclerosis lesion volume using stereotactic space, Proc. 4^{th} Vis. Biomed. Comp. (VBC), Hamburg, Germany.
19. Jacobsen LK, Rapoport JL (1998). Research update: childhood-onset schizophrenia: implications of clinical and neurobiological research. J. Child Psychol. Psychiatry. 1998 Jan;39(1):101-13.
20. Talairach J, Tournoux P (1988). Co-planar Stereotaxic Atlas of the Human Brain, New York: Thieme.
21. MacDonald D (1998). A Method for Identifying Geometrically Simple Surfaces from Three Dimensional Images, PhD Thesis, McGill Univ., Canada.
22. Ono M, Kubik S, Abernathey CD (1990) Atlas of the Cerebral Sulci. Stuttgart: Thieme.

23. Davatzikos C (1996). Spatial Normalization of 3D Brain Images using Deformable Models, J. Comp. Assist. Tomogr. 20(4):656-665, Jul.-Aug. 1996.
24. Fischl B, Sereno MI, Tootell RBH, Dale AM (1999). High-Resolution Inter-Subject Averaging and a Coordinate System for the Cortical Surface, Hum Brain Mapp. 8(4):272-84.
25. Thompson PM, Toga AW (1996). A Surface-Based Technique for Warping 3-Dimensional Images of the Brain, IEEE Transactions on Medical Imaging, 15(4):1-16.
26. Xu C, Pham DL, Rettmann ME, Yu DN, Prince JL (1999).Reconstruction of the human cerebral cortex from magnetic resonance images, IEEE Trans Med Imaging. 1999 Jun;18(6):467-80.
27. Thompson PM, Toga AW (2000). Elastic Image Registration and Pathology Detection, Bankman I et al. [eds.], Handbook of Medical Image Processing, Academic Press.
28. Burke WL (1985). Applied Differential Geometry, Cambridge University Press.
29. Joshi SC, Miller MI, Christensen GE, Banerjee A, Coogan TA, Grenander U (1995). Hierarchical Brain Mapping via a Generalized Dirichlet Solution for Mapping Brain Manifolds, SPIE 2573:278-289.
30. Liseikin VD (1991). On a Variational Method for Generating Adaptive Grids on N-Dimensional Surfaces, Doklady Akademii Nauk. CCCP, 1991, V319 N3:546-549.
31. Alouges F (1997). A New Algorithm For Computing Liquid Crystal Stable Configurations: The Harmonic Mapping Case, SIAM J. Num. Analysis 34(5):1708-1726.
32. Polyakov AM (1987). Gauge Fields and Strings. Harwood, New York.
33. Bakircioglu M, Joshi S, Miller MI (1999). Landmark Matching on Brain Surfaces via Large Deformation Diffeomorphisms on the Sphere, Proc. SPIE Medical Imaging.
34. Thompson PM, Moussai J, Khan AA, Zohoori S, Goldkorn A, Mega MS, Small GW, Cummings JL, Toga AW (1998). Cortical Variability and Asymmetry in Normal Aging and Alzheimer's Disease, Cerebral Cortex 8(6):492-509, Sept.1998.
35. Woods RP, Dapretto M, Sicotte NL, Toga AW, Mazziotta JC (1999). Creation and use of a Talairach-compatible atlas for accurate, automated, nonlinear intersubject registration, and analysis of functional imaging data. Hum Brain Mapp. 8(2-3):73-9.
36. Thirion J-P, Prima S, Subsol S (2000). Statistical Analysis of Dissymmetry in Volumetric Medical Images, Medical Image Analysis 4(2):111-121.
37. Cao J, Worsley KJ (2001). The Geometry of the Hotelling's T-squared Random Field with Applications to the Detection of Shape Changes, Annals of Statistics [in press].
38. Worsley KJ, Andermann M, Koulis T, MacDonald D, Evans AC (1999). Detecting changes in nonisotropic images. Hum Brain Mapp. 8(2-3):98-101.
39. Thompson PM, Mega MS, Narr KL, Sowell ER, Blanton RE, Toga AW (2000). Brain Image Analysis and Atlas Construction, Chapter, in: Fitzpatrick M [ed.], SPIE Handbook on Medical Image Analysis, SPIE Press.